Applied Catalysis B: Environmental 183 (2016) 394–406

Contents lists available at ScienceDirect

Applied Catalysis B: Environmental

journal homepage: www.elsevier.com/locate/apcatb

A kinetic model for sulfur poisoning and regeneration of Cu/SSZ-13 used for NH_3-SCR

Louise Olsson[a,*], Kurnia Wijayanti[a], Kirsten Leistner[a], Ashok Kumar[b], Saurabh Y. Joshi[b], Krishna Kamasamudram[b], Neal W. Currier[b], Aleksey Yezerets[b]

[a] Chemical Engineering, Competence Centre for Catalysis, Chalmers University of Technology, SE-412 96 Göteborg, Sweden
[b] Cummins Inc., 1900 McKinley Avenue, MC 50183, Columbus, IN 47201, USA

ARTICLE INFO

Article history:
Received 4 August 2015
Received in revised form 29 October 2015
Accepted 3 November 2015
Available online 10 November 2015

Keywords:
Kinetic model
Ammonia-SCR
Sulfur poisoning
Cu/SSZ-13
Cu-zeolites

ABSTRACT

In this study, we have developed a multi-site kinetic model that describes the sulfur poisoning and gradual sulfur removal over Cu/SSZ-13 used for NH_3-SCR. Sulfur poisoning was conducted under SCR conditions and thereafter, repeated SCR experiments were conducted to examine the effect of such poisoning and the subsequent gradual removal of sulfur. In addition, the effect of sulfur poisoning was examined on NH_3 TPD and ammonia oxidation experiments. The following sites were used in the kinetic model: copper in the six-membered rings as described by $S1_{Cu}$, copper in the larger cages with S2 and S3 as a site where physisorbed ammonia can attach. Further, ammonia was also adsorbed on the Brönsted sites, represented by $S1_{Brön}$ in the model, but in order not to further complicate the model, small amounts of ammonia storage on Brönsted sites were also lumped into S2. In the model, SO_2 was adsorbed on the sites containing copper, which are $S1_{Cu}$ and S2. It should be noted that $S1_{Cu}$ and S2 represents hydrated copper sites. Interestingly, we observed experimentally that ammonia storage was larger after sulfur poisoning compared to before, which is why we added ammonia storage and desorption to the $S1_{Cu}$–SO_2 and S2–SO_2 sites. However, ammonia was already adsorbing on the copper site; thus, these steps did not result in increased storage. Consequently, reaction steps were added where additional ammonia was adsorbed to form $S1_{Cu}$–SO_2–$(NH_3)_2$ and S2–SO_2–$(NH_3)_2$ species, which could be interpreted as precursors to ammonium sulfates. Another aspect that must be addressed in the model is the observation in the literature that SO_2 is more easily desorbed in $SO_2 + NH_3 + O_2$ TPD than $SO_2 + O_2$ TPD. Reversible reaction steps were therefore added whereby the $S1_{Cu}$–SO_2–NH_3 and S2–SO_2-NH_3 species were decomposed to form SO_2. A final reaction step was incorporated into the model to describe the SCR reaction with ammonia attached to the sulfur sites. The developed model could well describe the sulfur poisoning and gradual regeneration during repeated SCR experiments. In addition, the model well described the NH_3 TPD and NH_3 oxidation before and after sulfur poisoning.

1. Introduction

Ammonia based selective catalytic reduction (SCR) is an important technique for reducing NO_x from diesel and lean-burn gasoline vehicles. A significant amount of research has been conducted over the years regarding NH_3-SCR using several different catalyst types, of which vanadia on titania [1–5], Fe-exchanged zeolites [6–8] as well as Cu-zeolites [9–13] have been the major catalytic groups. The copper-zeolites possess higher low temperature activity than the iron-exchanged zeolites [14], which is a major advantage. In the last few years, the small-pore copper-zeolites have received great attention due to their high activity in combination with high hydrothermal stability and resistance to hydrocarbon poisoning [15]. The focus of the small-pore zeolites/ silicoaluminophosphates has been on materials with a chabazite (CHA) structure, such as Cu/SAPO-34 [11,16,17] and Cu/SSZ-13 [12,15,17–19]. The copper loading plays a critical role for the activity and selectivity of the material and it was found that the rate for oxidation reactions for both Cu/BEA [20] and Cu/SSZ-13 [21] were larger on the over-exchanged copper zeolites, whereas the opposite results were found for the SCR reaction. In conclusion, there are at least two different types of copper species present in the copper exchanged zeolites [20]. For Cu/SSZ-13, results from several studies [10,22,23] suggest that copper is preferentially ion-exchanged into sites in the six-membered rings, which might be slightly distorted due to interactions with water and ammonia [24]. For higher loading, the

* Corresponding author. Fax: +46 31 772 3035.
E-mail address: louise.olsson@chalmers.se (L. Olsson).

http://dx.doi.org/10.1016/j.apcatb.2015.11.001
0926-3373/

Nomenclature

A_i	Pre-exponential factor for reaction i (s^{-1})
d_{hyd}	Hydraulic diameter of the channel (m)
$E_{A,i}$	Activation energy for reaction i (J/mol)
$E^0_{A,i}$	Activation energy for reaction i at zero coverage (J/mol)
GSA	Geometric surface area per reactor volume (m^{-1})
$k_{k,m}$	Mass transfer coefficient of species k (mol/m^2 s)
k_i	Rate constant for reaction i (s^{-1})
$MG_{k,G}$	Molar mass of gas phase species k (kg/kmol)
r_i	Reaction rate for reaction i (kmol/(s m^2))
T_s	Temperature at catalyst surface (K)
t	Time (s)
v_g	Gas velocity (m/s)
$\nu_{i,k}$	Stoichiometric coefficient of species k in reaction i (−)
$w_{k,g}$	Mass fraction of species k in gas phase (−)
y_k	Mole fraction at the reaction layer of specie k (−)
y^B_k	Mole fraction in the gas bulk of specie k (−)
z	Spatial coordinate in axial direction (m)

Greek letters

α_i	Coverage dependence in reaction i (−)
ϵ_g	Volume fraction of gas phase in entire system (−)
θ_k	Coverage of species k (−)
ρ_g	Density of the gas phase (kmol/m^3)
Ω_j	Surface site density of storage site j (kmol/m^2)

copper is starting to be ion-exchanged into large cages [9,24] or is forming Cu_xO_y species [10]. It is proposed that the main SCR activity in Cu/SSZ-13 derives from the copper in the six-membered rings.

Sulfur is always present in the exhausts from vehicles and it is therefore critical to study the effect of sulfur on the activity and selectivity of the catalytic system. It has previously been found that vanadia based SCR catalysts deactivate to a lesser degree after being exposed to sulfur than metal-zeolite SCR catalysts [25–27]. Further, the copper species are more susceptible to sulfur poisoning than Fe-zeolites [25,28,29]. However, according to a study by Schmieg and Lee [25], for copper-zeolites it is possible to decrease the effect of the poisoning if fast SCR conditions compared to standard SCR were applied. These results were also found in one of our earlier studies [11] using Cu/SAPO-34, in which we also observed that there was less sulfur deactivation when using 50% NO_2 compared to standard SCR conditions. Further, the poisoning was even less when using 75% NO_2 instead of 50% in the feed. The main reason for the deactivation of Cu/zeolites is that sulfur attaches to the copper sites. XRF studies by Zhang et al. [30] showed that there was almost no sulfur present on the SAPO-34 support; thus, the sulfur mainly attaches to the copper sites. We previously observed this result by the decreased reducibility of the copper during TPR of Cu/SAPO-34 after SO_2 exposure [11]. In the case when ammonia was present during the sulfur poisoning, ammonium sulfates were primarily formed [31] and started to decompose at 300 °C. Further, when the catalyst was treated at high temperature, the activity resumed [31]; however, a temperature of 500 °C under SCR conditions would be insufficient to fully regenerate the Cu/SAPO-34 although parts of the activity would resume. Further, Kumar et al. [32] observed that the sulfur poisoning was more severe if the Cu-zeolite was exposed to SO_3 rather than to SO_2 at high poisoning temperature (400 °C), but this was not the case at 200 °C. In addition, SO_3 exposure resulted in a poisoning that was more difficult to regenerate [32].

In the literature, there are many kinetic models for NH_3-SCR that are using different catalysts, for example vanadia on titania [1–5], Cu/ZSM-5 [33–36], Cu/FAU [37], Cu/BEA [38], Cu/CHA [39], Cu/SSZ-13 [12], HZSM-5 [40] and Fe/zeolites [6–8,41]. Both detailed [12,34–36], as well as global kinetic models [33,42,43] have been developed for Cu/zeolites. The ammonia storage and release form a critical part of the kinetic model in order to capture transient effects. For this purpose, micro-calorimetry can be a great help with which to measure the heat of adsorption [44] and thereafter use in the kinetic model [38]. Wilken et al. [44] developed a method for retrieving the coverage-dependent heat of adsorption of ammonia for Cu/BEA at atmospheric pressure [44]. This method resulted in a linear trend in accordance with the Temkin isotherm, which has been successfully used in many modeling studies [5,7,33,35,45]. There are both single-site models [33,38], as well as multiple-site models [8,12,35,46,47]. In general, if a large temperature interval is used, a multiple-site model is often needed. In a recent study, we developed a kinetic model for ammonia storage, oxidation and SCR using a well-characterized Cu/SSZ-13 catalyst [12]. In order to describe ammonia storage/release simultaneously with the activity over a broad temperature interval, a three-site model was needed [12]. But, there are limited studies available in the literature that present kinetic models for the aging of copper-zeolites used for the ammonia-SCR reaction. Actually, the only available model for the aging of Cu zeolites used for NH_3 SCR is to our knowledge our previous model that described the hydrothermal aging of Cu/BEA [38].

However, there are no kinetic models in the literature that can describe the sulfur poisoning and regeneration during NH_3-SCR. The objective of this study has been to develop a kinetic model capable of describing the sulfur poisoning and gradual regeneration during NH_3-SCR using a well-characterized Cu-SSZ-13 catalyst.

2. Experimental

2.1. Catalyst synthesis and characterization

The same monolith with Cu/SSZ-13 as was used for the experiments that formed the basis for the multiple-site kinetic model for the fresh catalyst [12] has been used in the present study. The procedure for synthesizing the Cu/SSZ-13 powder has been described in detail in the former publication [12]. The powder was used to coat a monolith (400 cpsi) of the dimensions 20 mm in length and 21 mm in diameter. In order to increase the attachment of the zeolite, a thin layer of alumina (Disperal P2, Sasol, GmbH) was first added (67 mg). Thereafter, the monolith was stepwise coated with the zeolite, where Boehmite was used as a binder when coating the zeolite layer, with a ratio 95/5 between zeolite and binder. The resulting zeolite layer was 780 mg in a sample of total wash coat amount of 847 mg.

The powder was characterized using XRD in order to ensure the CHA-structure, using a Bruker AXS. The catalyst was further characterized using BET (Micromeritics ASAP 2010) resulting in a surface area of 439 m^2/g and a pore volume of 0.22 cm^3/g. The elemental analysis was conducted using ICP-SFMS, which yielded a Cu-loading of 3.1 wt.%, and a Si/Al ratio of 3.56. In addition, residues of sodium (1.57 wt.%) and iron (0.06 wt.%) from the preparation of the SSZ-13 were found in the powder. Details regarding catalyst characterization, such as XRD, BET, ICP-SFMS and TPR, can be found in Ref. [48].

2.2. Flow reactor experiments

Details regarding the flow reactor equipment used in this study can be found in earlier studies [11]. Briefly, the monolith catalyst

was placed in a quarts reactor, with one thermocouple measuring the temperature in the center channel and a second thermocouple used for controlling the temperature in the gas phase before the catalyst. Gases were mixed using multiple mass flow controllers (Bronkhorst) and water was added with a Bronkhorst CEM (Controlled Evaporation and Mixing) system. The gases were analyzed using an FTIR spectrometer (MKS Multigas 2030). The total flow was 3500 ml/min, resulting in a space velocity based on a monolith volume of 30,300 h^{-1} with Ar used as an inert balance.

First, the catalyst was degreened using 400 ppm NH_3, 400 ppm NO, 8% O_2 and 5% H_2O at 650 °C for 4 h. Prior to all experiments involving the fresh catalyst, it was pre-treated with 8% O_2 and 5% H_2O for 20 min at 600 °C. The experimental procedure for the experiments conducted over the fresh catalyst was as follows. An ammonia temperature programmed desorption (TPD) experiment was performed over the fresh catalyst for characterizing the storage and release of ammonia from the catalyst. For this experiment, the catalyst was exposed to 400 ppm NH_3 and 5% H_2O for 90 min at 50 °C, followed by flushing the sample with 5% H_2O in Ar for 80 min. Thereafter, the temperature was increased to 600 °C with a ramp speed of 10 °C/min, while exposing the catalyst to the same gas mixture. The ammonia oxidation was examined by exposing the catalyst to 400 ppm NH_3, 8% O_2 and 5% H_2O and increasing the temperature in steps from 150 to 600 °C. Finally, ammonia SCR was investigated by exposing the catalyst to 400 ppm NH_3, 400 ppm NO, 8% O_2 and 5% H_2O, and by increasing the temperature stepwise from 100 to 600 °C.

The catalyst was thereafter poisoned at 300 °C for 90 min by exposing it to 30 ppm SO_2, 400 ppm NH_3, 400 ppm NO, 8% O_2 and 5% H_2O. Thereafter, eight ammonia-SCR experiments were conducted in a sequence, with no additional sulfur poisoning in-between the experiments. The first SCR experiment after poisoning was denoted SCR1, the second SCR2, etc. During these experiments, the catalyst was exposed to 400 ppm NH_3, 400 ppm NO, 8% O_2 and 5% H_2O starting at 100 °C and increasing the temperature in steps to 400 °C. The objective of conducting the experiments to only 400 °C was to study the gradual removal of the sulfur during repeated experiments at medium temperatures. After these eight experiments, stable conversion was reached and experiments for examining ammonia oxidation and ammonia storage were conducted. The ammonia oxidation experiment was similar to the experiment conducted for the fresh catalyst except for the difference of using 400 °C as the maximum temperature compared to 600 °C for the fresh catalyst. Correspondingly, a comparable procedure was used for the ammonia TPD after sulfur poisoning as for fresh, but reaching only 400 °C in the ramp. The pre-treatment prior to all experiments for the sulfur-treated catalyst, except the first SCR experiment after poisoning, was to expose the catalyst to 8% O_2 and 5% H_2O at 400 °C for 20 min. For the first SCR experiment after sulfur poisoning (SCR1), no pre-treatment was used.

3. Kinetic modeling

3.1. Reactor model

AVL BOOST, version 2013 [49], was used for conducting the kinetic simulations. One channel was used for the calculations, which was axially discretized into 20 grid points, with uniform size and in addition, the mass-transfer in the washcoat was resolved using five grid-points. The main governing equation for the gas phase species was:

$$\epsilon_g \frac{\partial \rho_g \times w_{k,g}}{\partial t} = \epsilon_g \frac{\partial \rho_g \times w_{k,g} \times v_g}{\partial z} + MG_{k,g} \sum_i^{nr} v_{i,k} \times r_i \left(y_k, T_s, \theta_k\right) \quad (1)$$

The corresponding equation for the coverage of component k on the surface was:

$$\frac{\partial \theta_k}{\partial t} \left(\Theta \times GSA\right) = \sum_i^{nr} v_{i,k} \times r_i \left(y_k, T_s, \theta_k\right) \quad (2)$$

GSA, the geometric surface area per unit reactor volume, is determined by:

$$\frac{GSA}{d_{hyd}} = 4 \times (\text{cell density}) \quad (3)$$

In a monolithic system, it is important to describe the mass-transfer. The film model was used for simulating the external mass transport from the gas bulk to the surface according to:

$$GSA \times k_{k,m} \times \left(y_k - y_k^B\right) = \sum_i^{nr} v_{i,k} \times r_i \left(y_k, T_s, \theta_k\right) \quad (4)$$

In addition to the external mass-transfer, the mass-transfer in the washcoat was calculated using a constant pore diffusion model, with an effective diffusivity of 5×10^{-6} m^2/s for the different components, in accordance with Chatterjee et al. [50]. The reaction heat associated with the reactions in the SCR mechanism is very low and therefore, the heat balances were not resolved. This approach has been applied in many models presented in the literature [8,12,33–36,38,51]. The temperature measured inside the center channel of the catalyst was used in the simulations (except for the poisoning at 300 °C where the set value of 300 °C was used).

3.2. Kinetic model

The rate constants are described using the Arrhenius equation according to:

$$k_i = A_i e^{\frac{-E_{A,i}}{(RT_s)}} \quad (5)$$

Ammonia adsorption and desorption are crucial reactions in order to describe the transient effects for a kinetic model involving SCR. Using micro-calorimetry, we have previously found that the heat of adsorption, ΔH, for ammonia adsorption on Cu/BEA is a linear function of the ammonia coverage [44]. This is indeed the form of the Temkin isotherms that have been used for describing the ammonia desorption in many kinetic models [5,7,33,35,45]. If assuming ammonia adsorption as non-activated, which is the case in many studies [12,52], it would result in the following activation energy for ammonia desorption:

$$E_{A,i} = E_{A,i}^0 \left(1 - \alpha_i \times \theta_{S1-NH_3}\right) \quad (6)$$

The current model for sulfur poisoning and regeneration is based on a newly developed multi-site kinetic model for Cu/SSZ-13 [12]. The same Cu/SSZ-13 monolith as in the SCR experiments in our previous paper [12] was actually used for the current sulfur-poisoning experiments. Thus, all parameters from the multi-site model have remained fixed in the current study. The previously developed model [12] will first be briefly described. The multi-site kinetic model contains three sites denoted S1, S2 and S3. Based on experiments with varying copper loading using both Cu/BEA [20] as well as Cu/SSZ-13 [21], there were two types of active copper species present, where the over-exchanged sites were mainly responsible for the oxidation reactions and the SCR reaction occurred preferentially on the under-exchanged sites. In addition, it has been found earlier using Fe/zeolites that it is important to have an additional SCR reaction occuring at high temperature, when the ammonia coverage on the main storage sites becomes very low [8]. Further, both copper and Brönsted acid sites are well-known to store ammonia and the contributions from both copper and Brönsted sites were

initially lumped together in S1 and S2 in order not to further complicate the model. This approach has been successfully used in many previous models [33,38,53–56]. The physical interpretation of the sites used in the model is:

- S1 is the main storage site for NH_3. For Cu/SSZ-13, copper is first ion-exchanged into sites located in the six-membered rings [10,22,23]. Since the catalyst used in this study is under-exchanged, we suggest that the copper contributing to the main site, S1 is located in the six-membered rings. Initially, as described above, the storage on the acid sites are lumped together with the copper sites in order not to further complicate the model. However, as will be thoroughly discussed in Section 4, it would actually be crucial for the sulfur-poisoning model to separate the storage on the Brönsted and copper sites which is why in the latter simulations, S1 was divided into:

  – $S1_{Cu}$: the copper species contributing to the S1 site.
  – $S1_{Brön}$: the Brönsted acid sites contributing to the S1 site.

- S2 represents sites that store ammonia at high temperature. We found earlier that for both Cu/BEA and Cu/SAPO-34, there was increased ammonia desorption at high temperature visible in the TPD when the copper loading was increased [20,57]. In addition, Gao et al. [24] and Kwak et al. [9], proposed that for higher copper loadings, copper would occupy the sites in the large cages. We therefore suggest that the copper contributing to S2 is associated with the larger cages. In addition, as described above, some ammonia storage on Brönsted sites are lumped into the S2 sites in order to simplify the model.

- S3: is the site for physisorbed ammonia, which occurs at low temperature.

It should be noted that in zeolites there are large amount of water present [35] and Wilken et al. [58] found that copper in Cu/BEA is in the form of copper hydroxyls, according to UV–vis experiments. Furthermore, McEwen et al. [59] observed that copper in Cu/SSZ-13 stored in air at RT behaves like fully hydrated copper ($[Cu(II)(H_2O)_6]^{2+}$) using XANES, and the importance of water interactions in Cu/SSZ-13 were supported by DFT calculation, where $ZCu(II)(OH)_2$, $Z_2Cu(II)OH_2$ and $ZCu(I)OH_2$ were found to be the most stable species [59]. In all experiments used for developing the kinetic model, high water concentration was present (5%). Thus, very likely there are water or OH groups interacting with copper in our Cu/SSZ-13. However, since all experiments contain water and in order to not further complicate the model, the water interactions have not been modeled in detail. The $S1_{Cu}$ and S2 sites therefore represent hydrated sites.

Table 1 depicts the reactions and corresponding rates for the multi-site SCR model [12]. The first three reactions describe the storage and release of ammonia on the three sites. It should be noted that it is possible that multiple ammonia molecules could be stored on each copper site. For example, Giordanino et al. [60] proposed based on XANES O_{fw}–C_u–NH_3 and H_3N–Cu–NH_3 species and Moreno-González et al. [61] proposed that one, three and five NH_3 molecules can bind to the copper site. However, in order not to complicate the model, we have used adsorption of one ammonia molecule to each site. Ammonia oxidation is often occurring at high temperature [13] and is associated with over-exchanged Cu-sites [20]; we therefore propose that the main ammonia oxidation would occur on S2 sites which is illustrated in Eq. (5), Table 1. However, it was also experimentally observed that small amounts of ammonia could be oxidised at low tempeature and, therefore, an ammonia oxidation reaction was introduced on S1. This reaction was critical in order to explain the complex behavior of ammonia oxidation occurring over Cu/SSZ-13 [12], whereby the ammonia conversion reached a minimum at 400 °C and thereafter increased again. During ammonia oxidation only minor formation of N_2O (maximum 3 ppm) and NO (maximum max 5 ppm) was observed and therefore were no reactions added for these steps. Moreover, the NO oxidation reaction was not included, because NO oxidation was very low over these samples, reaching only about 4% conversion at 400 °C [48]. In addition, it was found using DRIFT spectroscopy over Cu/ZSM-5 that the coverage of nitrites/nitrates decreased in the presence of NH_3 due to ammonia inhibition [62]. It is therefore probable that ammonia also inhibits the NO oxidation, resulting in even lower NO oxidation in SCR conditions.

Furthermore, ammonia SCR was observed to occur more rapidly at lower ion-exchange levels for both Cu/BEA [20] and Cu/SSZ-13 [21]. We therefore suggested that the main SCR reaction occurs on S1 sites [12] (see Reaction (6), Table 1). However, similarly as in the kinetic model for Fe/zeolites [8], the coverage of ammonia on the main storage site, in our case S1, was low at high temperature, resulting in an activity for ammonia SCR at high temperature that was too low. We therefore introduced a reaction step for ammonia SCR on S2 sites as well, which is described by Reaction (7) in Table 1. Further, it is critical to describe the N_2O formation in a kinetic model; for both Cu/SSZ-13 [12] and Cu/BEA [20], the N_2O production possessed several interesting experimental features. At low temperature, the N_2O formation went through a maximum, which was often related to the formation and decomposition of an ammonium nitrate type of species [20,63]. For standard SCR conditions, no NO_2 was available in the inlet feed and NH_3-NO species were suggested to be formed, which might be precursors to ammonium nitrate species. This mechanism was used for both Cu/BEA [38] and Cu/SSZ-13 [12] in our earlier kinetic models and was in the current study modelled according to Reactions (8)–(9), Table 1. Finally, since N_2O formation again started to increase above 450 °C (see Reaction (10), Table 1), the last step of the kinetic model for the fresh system was a step involving N_2O production at high temperature. High temperature N_2O formation has been experimentally observed over Cu/BEA [13], Cu/FAU [64], Cu/SSZ-13 [12] and Cu/SAPO-34 [57]. Delahay et al. [64] suggested that above 600K, the N_2O formation occurs on copper in the sodalite cages and this hypothesis is in line with our kinetic model for high temperature N_2O formation, where N_2O production occurs on the S2 sites, which represents copper species in the larger cages. At lower temperature Delahay et al. [64] propose that the N_2O formation originate from ammonium nitrate formation and decomposition on CuO species. Indeed, N_2O formation in standard SCR conditions occurred over CuO, as was shown by Centi et al. [65] using CuO/Al_2O_3. However, N_2O formation can also occur on other copper species and even on the acid sites. Leistner et al. [57] observed higher rate for N_2O formation during fast SCR conditions over H/SAPO-34 compared to the Cu/SAPO-34 samples. Furthermore, in our previous study over Cu/BEA, we observed increasing N_2O formation in standard SCR conditions when increasing the copper loading, even though UV–vis did not show any signs of CuO production [20]. In this study we propose that the N_2O reaction rate is higher for copper sites with higher exchange level and we therefore added the N_2O formation at low temperature on the S2 site as well, using a mechanism with NH_3-NO species.

The corresponding parameters are found in Table 2 and the tuned site densities were 81.1, 7.84 and 1.29×10^2 mol/(m^3 monolith). Details regarding fresh conditions for the model have been presented in an earlier publication [12].

After the initial sulfur model, it was critical to separate the contribution from copper in the six-membered rings and Brönsted acid sites in the S1 sites. Thus, we introduced $S1_{Cu}$ and $S1_{Brön}$ in order to capture the ammonia storage on copper and Brönsted sites, respec-

Table 1
Reactions and rate expressions for fresh ammonia SCR model [12].

Reaction	Reaction rate	Reaction number
$NH_3 + S1 \overset{r_1}{\Leftrightarrow} S1 - NH_3$	$r_{1f} = \Psi_{S1} k_{1,f} y_{NH_3} \theta_{S1}$ $r_{1b} = \Psi_{S1} k_{1,b} \theta_{S1-NH_3}$	(1)
$NH_3 + S2 \overset{r_2}{\Leftrightarrow} S2 - NH_3$	$r_{2f} = \Psi_{S2} k_{2,f} y_{NH_3} \theta_{S2}$ $r_{2b} = \Psi_{S2} k_{2,b} \theta_{S2-NH_3}$	(2)
$NH_3 + S3 \overset{r_3}{\Leftrightarrow} S3 - NH_3$	$r_{3f} = \Psi_{S3} k_{3,f} y_{NH_3} \theta_{S3}$ $r_{3b} = \Psi_{S3} k_{3,b} \theta_{S3-NH_3}$	(3)
$2S1 - NH_3 + 1.5O_2 \overset{r_4}{\Rightarrow} N_2 + 3H_2O + 2S1$	$r_4 = \Psi_{S1} k_4 y_{O_2}^{0.6} \theta_{S1-NH_3}$	(4)
$2S2 - NH_3 + 1.5O_2 \overset{r_5}{\Rightarrow} N_2 + 3H_2O + 2S2$	$r_5 = \Psi_{S2} k_5 y_{O_2}^{0.6} \theta_{S2-NH_3}$	(5)
$4S1 - NH_3 + 4NO + O_2 \overset{r_6}{\Rightarrow} 4N_2 + 6H_2O + 4S1$	$r_6 = \Psi_{S1} k_6 y_{NO} y_{O_2}^{0.5} \theta_{S1-NH_3}$	(6)
$4S2 - NH_3 + 4NO + O_2 \overset{r_7}{\Rightarrow} 4N_2 + 6H_2O + 4S2$	$r_7 = \Psi_{S2} k_7 y_{NO} y_{O_2}^{0.5} \theta_{S2-NH_3}$	(7)
$S2 - NH_3 + NO \overset{r_8}{\Leftrightarrow} S2 - NH_3 - NO$	$r_{8f} = \Psi_{S2} k_{8,f} y_{NO} \theta_{S2-NH_3}$ $r_{8b} = \Psi_{S2} k_{8,b} \theta_{S2-NH_3-NO}$	(8)
$2S2 - NH_3 - NO + O_2 \overset{r_9}{\Rightarrow} N_2O + N_2 + 3H_2O + 2S2$	$r_9 = \Psi_{S2} k_9 y_{O_2} \theta_{S2-NH_3-NO}$	(9)
$2S2 - NH_3 + 2NO + O_2 \overset{r_{10}}{\Rightarrow} N_2O + N_2 + 3H_2O + 2S2$	$r_{10} = \Psi_{S2} k_{10} y_{O_2} y_{NO} \theta_{S2-NH_3}$	(10)

Table 2
Parameters of the kinetic model for ammonia storage and release, ammonia oxidation, ammonia SCR and N_2O formation [12].

Reaction	Pre-exp. Factor, forward reaction (s^{-1})	Activation energy, forward reaction (kJ/mol)	Pre-exp. Factor, backward reaction (s^{-1})	Activation energy, backward reaction (kJ/mol)
1. NH_3 ads./desorption, S1	1.21×10^4	0.0	10^{13}	149.0[a,b]
2. NH_3 ads./desorption, S2	2.47×10^6	0.0	10^{13}	137.8[b]
3. NH_3 ads./desorption, S3	10.6	0.0	2.04	18.6
4. NH_3 oxidation, S1[d]	8.61×10^3	72.7[c]	–	–
5. NH_3 oxidation, S2	1.79×10^{12}	195.0	–	–
6. NH_3 SCR, S1[d]	4.83×10^8	68.3[c]	–	–
7. NH_3 SCR, S2	1.67×10^{11}	105.0	–	–
8. S2-NH_3–NO form./decomp.	3.30×10^7	63.0	2.68×10^{16}	145.0
9. N_2O formation from S2–NH_3–NO	2.49×10^7	35.0	–	–
10. High temp. N_2O formation	1.72×10^{11}	112.0	–	–

[a] $\alpha = 0.20$.
[b] Determined from micro-calorimetry.
[c] Determined from Arrhenius plot.
[d] For simulations when S1 is divided into $S1_{Cu}$ and $S1_{Brön.}$ A4 and A6 is multiplied with 1.7235 for compensating for the site density, giving A4=14.84×10^3 and A6 = 8.32×10^8.

tively. It would have been possible to divide the S2 sites as well. However, since the S2 sites contributed to only 9% of the S1 + S2 sites, dividing the S2 sites would not be critical to the model and was therefore left out in order not to further complicate the model. It should be noted that ammonia storage on extra-frame work Al is possible [66], but in order not to further complicate the model this is lumped together with the Brönsted acid sites. The updated storage mechanism is presented in Table 3.

In order to estimate the site density for $S1_{Cu}$ and $S1_{Brön}$, we determined the number of Cu atoms in the catalyst to be 380.5 μmol based on ICP-SFMS data [12]. Further, based on simulations of ammonia TPD from 50 °C, we received 561.9 and 54.2 μmol stored ammonia on S1 and S2, respectively. As an estimate, we assumed that the main part of S2 be attributed to copper sites and even though some of the storage on S2 is likely connected to Brönsted sites the error connected with this assumption is small due to the small storage on S2 compared to S1 (only 9% of the storage is occurring on S2 in the model). Using this simplification the amount of copper sites on S1 can be calculated to be 326.3 μmol (380.5–54.2 μmol). The remaining storage on S1 would be attributed to $S1_{Brön}$, resulting in $S1_{Cu}$ that would be 58% of S1 and correspondingly 42% would be associated with the acid sites ($S1_{Brön}$), i.e. the site density would be 47.0 and 34.1 mol/(m^3 monolith) for $S1_{Cu}$ and $S1_{Brön}$. In order to compensate for the difference in site density between $S1_{Cu}$ compared to S1, the pre-exponential factors for A4 and A6, given in Table 2, are multiplied by a factor (site density for S1 divided by site density for $S1_{Cu}$), as given in the Table footnote of Table 2.

Table 3
Updated ammonia storage mechanism.

Reaction	Reaction rate	Reaction number
$NH_3 + S1_{Cu} \overset{r_{1,Cu}}{\Leftrightarrow} S1_{Cu} - NH_3$	$r_{1f,Cu} = \Psi_{S1-Cu} k_{1,f} y_{NH_3} \theta_{S1_{Cu}}$ $r_{1b,Cu} = \Psi_{S1-Cu} k_{1,b} \theta_{S1_{Cu}-NH_3}$	(1-Cu)
$NH_3 + S1_{Brön.} \overset{r_{1,Brön.}}{\Leftrightarrow} S1_{Brön.} - NH_3$	$r_{1f,Brön.} = \Psi_{S1-Brön.} k_{1,f} y_{NH_3} \theta_{S1_{Brön.}}$ $r_{1b,Brön.} = \Psi_{S1-Brön.} k_{1,b} \theta_{S1_{Brön.}-NH_3}$	(1-Brön.)
$NH_3 + S2 \overset{r_2}{\Leftrightarrow} S2 - NH_3$	$r_{2f} = \Psi_{S2} k_{2,f} y_{NH_3} \theta_{S2}$ $r_{2b} = \Psi_{S2} k_{2,b} \theta_{S2-NH_3}$	(2)
$NH_3 + S3 \overset{r_3}{\Leftrightarrow} S3 - NH_3$	$r_{3f} = \Psi_{S3} k_{3,f} y_{NH_3} \theta_{S3}$ $r_{3b} = \Psi_{S3} k_{3,b} \theta_{S3-NH_3}$	(3)

Table 4
Reactions and rate expressions for sulfur poisoning and regeneration.

Reaction	Reaction rate	Reaction number
$SO_2 + S1_{Cu} \overset{r_{11}}{\Rightarrow} S1_{Cu} - SO_2$	$r_{11} = \Psi_{S1-Cu} k_{11} y_{SO_2} \theta_{S1_{Cu}}$	(11)
$SO_2 + S2 \overset{r_{12}}{\Rightarrow} S2 - SO_2$	$r_{12} = \Psi_{S2} k_{12} y_{SO_2} \theta_{S2}$	(12)
$S1_{Cu} - SO_2 + NH_3 \overset{r_{13}}{\Leftrightarrows} S1_{Cu} - SO_2 - NH_3$	$r_{13f} = \Psi_{S1-Cu} k_{13,f} y_{NH_3} \theta_{S1_{Cu}-SO_2}$ $r_{13b} = \Psi_{S1-Cu} k_{13,b} \theta_{S1_{Cu}-SO_2-NH_3}$	(13)
$S2 - SO_2 + NH_3 \overset{r_{14}}{\Leftrightarrows} S2 - SO_2 - NH_3$	$r_{14f} = \Psi_{S2} k_{14,f} y_{NH_3} \theta_{S2-SO_2}$ $r_{14b} = \Psi_{S2} k_{14,b} \theta_{S2-SO_2-NH_3}$	(14)
$S1_{Cu} - NH_3 + SO_2 \overset{r_{15}}{\Leftrightarrow} S1_{Cu} - SO_2 - NH_3$	$r_{15f} = \Psi_{S1-Cu} k_{15,f} y_{SO_2} \theta_{S1_{Cu}-NH_3}$ $r_{15b} = \Psi_{S1-Cu} k_{15,b} \theta_{S1_{Cu}-SO_2-NH_3}$	(15)
$S2 - NH_3 + SO_2 \overset{r_{16}}{\Leftrightarrow} S2 - SO_2 - NH_3$	$r_{16f} = \Psi_{S2} k_{16,f} y_{SO_2} \theta_{S2-NH_3}$ $r_{16b} = \Psi_{S2} k_{16,b} \theta_{S2-SO_2-NH_3}$	(16)
$S1_{Cu} - SO_2 - NH_3 + NH_3 \overset{r_{17}}{\Leftrightarrow}$ $S1_{Cu} - SO_2 - (NH_3)_2$	$r_{17f} = \Psi_{S1-Cu} k_{17,f} y_{NH_3} \theta_{S1_{Cu}-SO_2-NH_3}$ $r_{17b} = \Psi_{S1-Cu} k_{17,b} \theta_{S1_{Cu}-SO_2-(NH_3)_2}$	(17)
$S2 - SO_2 - NH_3 + NH_3 \overset{r_{18}}{\Leftrightarrow}$ $S2 - SO_2 - (NH_3)_2$	$r_{18f} = \Psi_{S2} k_{18,f} y_{NH_3} \theta_{S2-SO_2-NH_3}$ $r_{18b} = \Psi_{S2} k_{18,b} \theta_{S2-SO_2-(NH_3)_2}$	(18)
$2S1_{Cu} - SO_2 - (NH_3)_2 + 2NO + 0.5O_2 \overset{r_{19}}{\Rightarrow}$ $2S1_{Cu} - SO_2 - NH_3 + 3H_2O + 2N_2$	$r_{19} = \Psi_{S1-Cu} k_{19} y_{NO} y_{O2}^{0.5} \theta_{S1_{Cu}-SO_2-(NH_3)_2}$	(19)

Table 5
Parameters of the kinetic model for sulfur poisoning and regeneration.

Reaction	Pre-exp. Factor, forward reaction (s^{-1})	Activation energy, forward reaction (kJ/mol)	Pre-exp. Factor, backward reaction (s^{-1})	Activation energy, backward reaction (kJ/mol)
11. SO_2 ads., *S1Cu*	20.0	0.0	–	–
12. SO_2 ads., *S2*	5.0×10^2	0.0	–	–
13. $S1_{Cu}$–SO_2–NH_3 from $S1_{Cu}$-SO_2	1.21×10^4	0.0	1.0×10^{13}	149.0[a]
14. S2-SO_2–NH_3 from S2-SO_2	2.47×10^7	0.0	1.0×10^{13}	137.8
15. $S1_{Cu}$–SO_2–NH_3 from $S1_{Cu}$–NH_3	2.00×10^2	0.0	7.5×10^{13}	249.0[b]
16. S2-SO_2–NH_3 from S2-NH_3	5.00×10^3	0.0	5.0×10^{12}	249.0[b]
17 $S1_{Cu}$–SO_2–$(NH_3)_2$ form./decomp.	1.21×10^4	0.0	5.0×10^{12}	180.0[a]
18. S2-SO_2–$(NH_3)_2$ form./decomp.	2.47×10^7	0.0	1.4×10^{13}	145.0
19. SCR using $S1_{Cu}$–SO_2–$(NH_3)_2$	5.0×10^{15}	145.0	–	–

[a] $\alpha_{13} = 0.10$ and $\alpha_{17} = 0.35$ and is multiplied with the sum of coverages of all ammonia containing species on $S1_{Cu}$.
[b] $\alpha_{15} = \alpha_{16} = 0.20$ and is multiplied by the sum of coverages of all SO_2 containing species on $S1_{Cu}$ and S2, respectively.

The main objective of this study has been to develop a kinetic model for sulfur poisoning and regeneration. The final model is shown in Table 4 and the corresponding parameters can be seen in Table 5. The mechanism and reaction steps for these processes with regard to the experimental findings will be discussed thoroughly throughout Section 4.

3.3. Simulation approach

The simulation of sulfur poisoning and regeneration is a very transient system, whereby for example a gradual sulfur removal during the experiments is occurring. Therefore, all the simulations were consequently performed in one overall simulation. The simulations were conducted in the following order: SO_2 poisoning in SCR conditions at 300 °C for 90 min, SCR1, SCR2, SCR3, SCR4, SCR5, SCR6, SCR7, SCR8, NH_3 TPD and, finally, NH_3 oxidation. Cooling steps between the experiments were added to the simulation in order to avoid sudden temperature steps, which might trigger numerical issues. The simulations for the fresh catalyst were performed separately.

4. Results and discussion

4.1. Kinetic model for ammonia SCR

The multiple site model, developed in an earlier study [12], is used for simulating an ammonia SCR experiment during which the temperature was increased in steps from 100 to 600 °C. During this experiment, the catalyst was exposed to 400 ppm NH_3, 400 ppm NO, 8% O_2 and 5% H_2O. The resulting steady state values for NO and NH_3 conversions are shown in Fig. 1a and b, respectively. In addition, the N_2O concentration is depicted in Fig. 1c. At low temperature, the conversion was close to 0, and thereafter gradually increased to reach a conversion of 95% at about 200 °C and then full conversion at 250 °C. At higher temperature, starting at about 350 °C, the NO conversion decreased slightly due to ammonia oxidation [20]. This is evident by the fact that 100% NH_3 conversion was reached at high temperature. However, the decrease in NO conversion was quite small because the Cu/SSZ-13 sample used was under-exchanged. It was observed that ammonia oxidation for Cu/BEA [20] preferentially occurred on copper sites formed on over-exchanged sites which explained the low ammonia oxidation of the current sample. The N_2O concentration (Fig. 1c) showed a complex behavior with a low temperature maximum, which the model well predicted. The low temperature N_2O is suggested to be related to the formation of NH_3-NO species, which is described by Reactions (8)–(9), Table 1, in the model. At higher temperature, the NH_3-NO species were decomposed, resulting in a lower coverage for these species, thereby decreasing the N_2O concentration. At even higher temperatures, the N_2O concentration again increased as predicted by the model based on Reaction (10), in Table 1. To conclude, the model well described the NO, NH_3 and N_2O concentrations over the entire temperature interval examined from 100 to 600 °C.

4.2. Simple sulfur storage model

Firstly, a simple sulfur-poisoning mechanism was tried where SO_2 was attached to the S1 and S2 sites (Eqs. (7) and (8)).

$$SO_2 + S1 \overset{r_{SO_2-1}}{\Rightarrow} S1 - SO_2 \quad (7)$$

$$SO_2 + S2 \overset{r_{SO_2-2}}{\Rightarrow} S2 - SO_2 \quad (8)$$

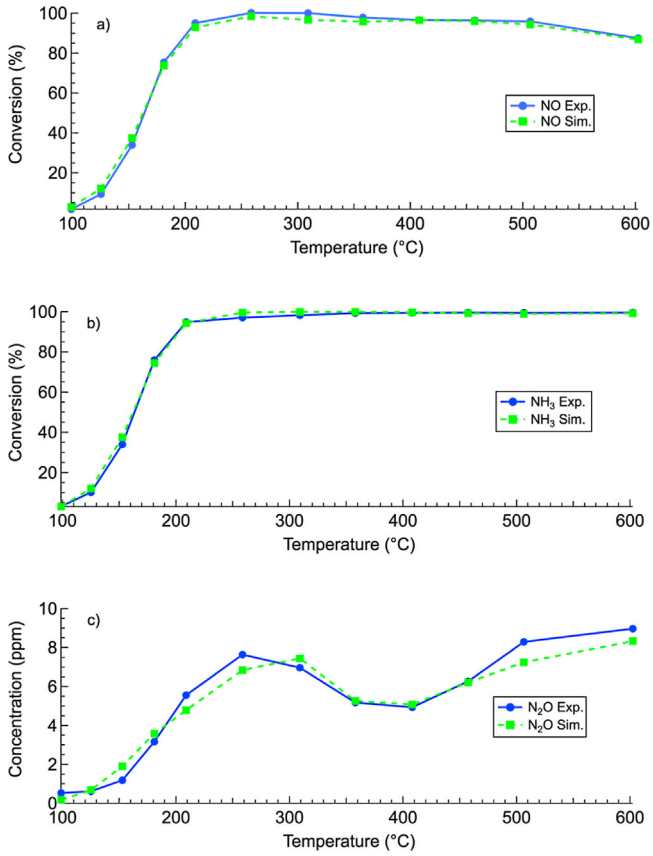

Fig. 1. Experiment and simulation of ammonia SCR when exposing the catalyst to 400 ppm NO, 400 ppm NH_3, 8% O_2 and 5% H_2O, where the concentrations of (a) NO, (b) NH_3 and (c) N_2O are depicted. Reaction (1)–(10), Table 1 is used.

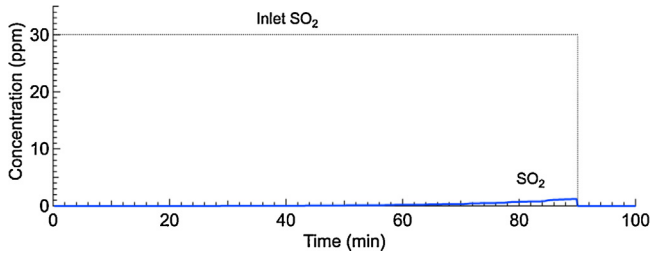

Fig. 2. Simulated SO_2 concentration during the poisoning step, with 30 ppm SO_2, 400 ppm NH_3, 40 ppm NO, 8% O_2 and 5% H_2O for 90 min at 300 °C.

with the corresponding rates

$$r_{SO_2-1} = \Psi_{S1} k_{SO_2-1} y_{SO_2} \theta_{S1} \quad (9)$$

$$r_{SO_2-2} = \Psi_{S2} k_{SO_2-2} y_{SO_2} \theta_{S2} \quad (10)$$

A high rate for SO_2 adsorption was used in order to simulate a severe poisoning situation and in Fig. 2, the simulated SO_2 concentration is shown from the poisoning step using 30 ppm SO_2, 400 ppm NH_3, 40 ppm NO, 8% O_2 and 5% H_2O for 90 min at 300 °C. Indeed, a rapid adsorption followed, resulting in an almost total uptake of all SO_2 during the poisoning.

As described in Section 3.3 entitled Simulation approach, the simulations were conducted in one large sequence; thus, following the poisoning simulation, SCR1 was simulated (SCR1 denotes the first SCR experiment after sulfur poisoning). The results from the experiment, as well as the simulation of SCR1, are shown in Fig. 3. In addition, results for simulations and experiments for a fresh catalyst up to 300 °C are added to Fig. 3. The reason why the data for the fresh catalyst are not given at the highest temperatures where

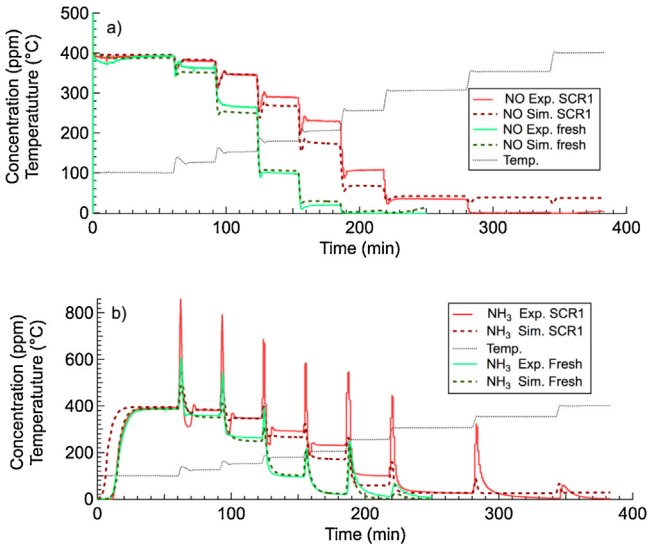

Fig. 3. Experimental and simulated results for SCR1 (first SCR experiment after sulfur poisoning) for (a) NO and (b) NH_3. In addition, simulations for the fresh catalyst are added up to 300 °C. The highest temperature steps were not added to the graph for the fresh catalyst due to shorter time intervals for these steps, but the results can be easily found in Fig. 1.

results for the poisoned catalyst are shown (see Fig. 3), is that the time intervals for these temperature steps was pro-longed after sulfur poisoning to ensure steady state conversion. However, the experimental and simulation results for the fresh catalyst at 350 and 400 °C can be easily seen in Fig. 1, where the NO conversion was 96 and 88% for 350 and 400 °C, respectively, and the conversion was 100% for NH_3. The results show that there is a large deactivation observed for NO (Fig. 3a) and NH_3 (Fig. 3b) after sulfur poisoning. However, the model significantly under-predicted the impact of the sulfur poisoning. The sulfur adsorption was already high, as seen by the large uptake of sulfur in Fig. 2. Thus, because almost all sulfur was already adsorbed on the catalyst, changing the parameters for this model would not improve the simulation results.

In the kinetic model, the copper and Brönsted acid sites are lumped together, which worked very well in simulating a fresh catalyst. However, SO_2 likely has a higher affinity to copper than the Brönsted acid sites [67], and the present model attaches sulfur to both copper and Brönsted acid sites. Indeed, Zhang et al. [30] found that by using XRF, almost no sulfur was attached to the SAPO-34 support; thus, the sulfur mainly attached to the copper sites. Further, in an earlier study, we found that the H_2 peak during the temperature programmed reduction experiment (TPR) decreased due to sulfur poisoning of Cu/SAPO-34 [11], which again showed that sulfur was attached to the copper sites. The model presented in this section needs further refinement in order to describe the sulfur storage on the copper sites and this will be described in the following section.

4.3. Advanced kinetic model for sulfur poisoning and regeneration

In order to incorporate into the model that SO_2 should be attached to copper only and not Brönsted sites, the S1 sites were divided into $S1_{Cu}$ and $S1_{Brön}$. Details about the estimated surface densities of these sites are described in detail in Section 3.2 entitled Kinetic model. Dividing S2 would have been possible without being crucial due to the low site density of S2 sites and was therefore not performed in order not to further complicate the model. Since the surface site densities were changed for the active copper sites, the pre-exponential factors for the SCR and ammonia oxidation reactions on S1 would have to be scaled, which is presented in

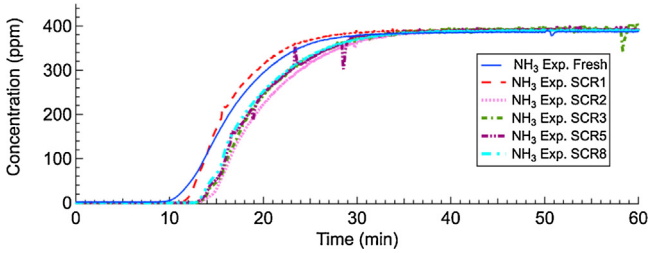

Fig. 4. NH_3 concentration during the first part of the SCR experiments at 100 °C for the fresh catalyst and after sulfur poisoning. SCR1: First experiment after poisoning, SCR2: Second experiment after poisoning, etc. The catalyst is exposed to 400 ppm NH_3, 400 ppm NO, 8% O_2 and 5% H_2O.

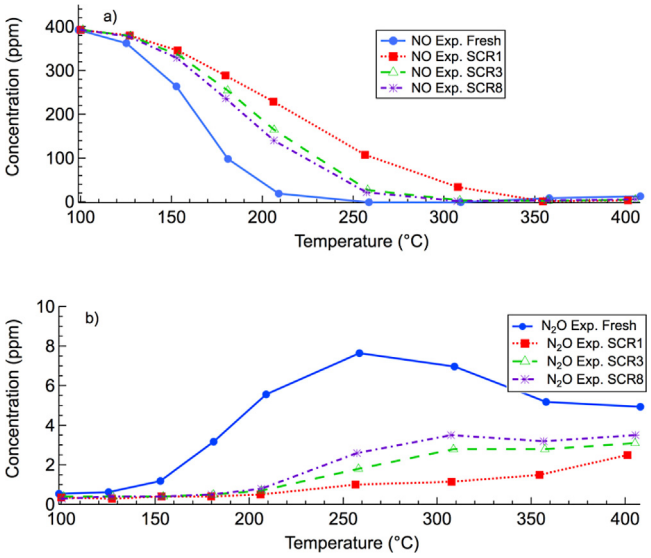

Fig. 5. SCR experiments, for fresh catalyst and after sulfur poisoning, where the (a) NO and (b) N_2O concentrations are shown. SCR1: First experiment after poisoning, SCR3: Third experiment after poisoning, etc. The catalyst is exposed to 400 ppm NH_3, 400 ppm NO, 8% O_2 and 5% H_2O.

Table 2. The updated model gives exactly the same results for the fresh catalyst as for the former model [12]. As described in earlier sections, the $S1_{Cu}$ and S2 sites represents hydrated copper sites. Therefore, SO_2 adsorption on a copper site with H_2O or OH groups attached to it could result in SO_2–OH or H_2SO_3 species. In order not to further complicate the model, we have chosen to denote the hydrated copper sites with $S1_{Cu}$ and S2 and do not model the interaction between the OH/H_2O and SO_2 in detail, but it should be noted that the OH/H_2O on the copper sites likely interacts with the SO_2.

When developing the poisoning mechanism, the NH_3 concentrations at 100 °C were examined for a variety of SCR experiments. In these experiments, the catalyst was exposed to SCR conditions (400 ppm NH_3, 400 ppm NO, 8% O_2 and 5% H_2O), but since the steady state conversion was close to 0% at this low temperature (see Fig. 1), it meant that the ammonia consumption was mainly related to the ammonia storage. In Fig. 4, the NH_3 concentration is shown for experiments involving the fresh catalyst and SCR experiments after sulfur poisoning, denoted SCR1 for the first SCR experiment after poisoning, SCR2 for the second experiment, etc. The ammonia outlet profile was similar for the fresh catalyst experiment and for the first experiment after sulfur poisoning (SCR1), which meant that they had similar ammonia storage. Interestingly, the ammonia storage was significantly higher on the second experiment after sulfur poisoning (SCR2) and remained similarly high for the following SCR experiments (SCR3–SCR8). In addition, the NH_3 TPD experiment conducted at 50 °C exhibited larger ammonia storage after sulfur poisoning. The fresh catalyst stored 1305 mmol NH_3 in the adsorption part of the TPD, whereas after sulfur poisoning the storage was increased by about 10% 1440 mmol. The NH_3 TPD results will be discussed in greater detail in connection with the model (Fig. 11). Our results are in accordance with the study conducted by Zhang et al. [31] who observed a larger storage of ammonia during $NH_3 + SO_2 + O_2$TPD than during $NH_3 + O_2$ TPD.

Prior to the our TPD experiments, the catalyst was pre-treated at 400 or 600 °C for a sulfur-poisoned and fresh sample, respectively, with 8% O_2 and 5% H_2O. During this pre-treatment, the major part of the ammonia adsorbed on the surface would be removed. However, the sulfur species are very stable and would likely remain on the catalyst during these pre-treatment conditions. Indeed, using ICP-SFMS we observed that after exposing the catalyst to SCR conditions up to 400 °C, the sulfur in the outlet part of the catalyst was not removed but in the inlet part of the catalyst, some sulfur was eliminated [48]. The reason for sulfur removal only in the inlet part of the monolith was likely due to the presence of SCR conditions, while in the outlet part the SCR reaction is nearly complete and only O_2 and H_2O were present. Thus, our results indicated that under O_2 and H_2O conditions, sulfur was not removed at 400 °C. Accordingly, when starting the ammonia TPD experiment over the sulfur-poisoned sample, the catalyst was free from ammonia but had a substantial amount of sulfur attached. We propose that ammonia can attach to these sulfur species and this is the reason for the increased ammonia storage of the sulfur-poisoned sample. This result also explains the increased ammonia storage between fresh catalyst and SCR2-SCR8 visible in Fig. 4. However, SCR1, i.e. the first experiment after sulfur poisoning, stores significantly less ammonia compared to subsequent SCR experiments. The reason is that sulfur poisoning was conducted under SCR conditions prior to this experiment. Thereafter, the temperature was lowered to 100 °C, without any pre-treatment. Thus, the catalyst still had ammonia from the poisoning at 300 °C on the surface, which lowered the ammonia storage in SCR1.

Another interesting aspect, which needs to be considered in developing the model, is the effect of the sulfur on the SCR reaction and the gradual removal of the sulfur. In Fig. 5, the NO (a) and N_2O (b) concentrations are shown for the fresh and sulfur-poisoned catalysts (SCR1, SCR3 and SCR8). It is clear that the sulfur poisoning significantly deactivated the catalyst, resulting in lower SCR functionality (compare fresh and SCR1, in Fig. 5a). In a similar way, the N_2O production was heavily decreased (see Fig. 5b). Interestingly, after repeated SCR experiments, some of the activity was regained as can be seen when comparing SCR1 and SCR3. Further, after several SCR experiments, a stable level was reached and it is evident from Fig. 5 that even though five consecutive SCR experiments were performed, the activity was only slightly improved between SCR3 and SCR8.

The experimental findings discussed in connection to Fig. 4 and 5, as well as in various literature findings, will form the basis for the development of the mechanism and kinetic model for sulfur poisoning and regeneration. From experimental studies, it is known that SO_2 can deactivate Cu/Zeolites, which was observed for Cu/SAPO-34 [11,31], Cu/SSZ-13 [48] and commercial Cu/CHA [32]. Since the activity decreased after sulfur poisoning, sulfur species must attach to the active copper sites. Further, using XRF, Zhang et al. [30] observed that there were almost no sulfur present on the SAPO-34 support; accordingly, the major part of the sulfur species were attached to the copper support. When exposing the Cu/SSZ-13 catalyst to only $SO_2 + O_2 + H_2O$ [48], we observed deactivation; thus, sulfur attaches to the catalyst without the presence of NO and NH_3. Based on these data, Reactions (11) and (12) in Table 4 were added where SO_2 could bind to the two copper sites, namely $S1_{Cu}$ and S2, respectively. It should be noted, as

discussed earlier, that $S1_{Cu}$ and S2 represents hydrated sites, thus e.g. $S1_{Cu}$–SO_2 can be interpreted as SO_2–OH or H_2SO_3 species on the copper sites. Direct sulfur removal is very difficult and indeed Zhang et al. [31] observed two desorption peaks during $SO_2 + O_2$ TPD over Cu/SAPO-34 at high temperature, around 550 and 680 °C. In the present study, the experiments after sulfur poisoning were conducted to a maximum of 400 °C, which was well under the desorption peak of SO_2, and therefore the SO_2 desorption step was not added to the model.

In the study by Zhang et al. [31], the lower desorption peak (550 °C) in the $SO_2 + O_2$ TPD was assigned to chemisorbed SO_2 forming sulfates and the high temperature peak (680 °C) was suggested to be associated with the decomposition of $CuSO_4$ or $Ce_x(SO_4)_y$ (the sample in Ref. [31] also contained ceria). Thus, there were likely different sulfur species present on the catalyst. These results are in line with the study by Kumar et al. [32], who observed a more severe deactivation after using SO_3 than after using SO_2 at 400 °C because more stable sulfates were formed when using SO_3. These results imply that during SO_2 exposure, the most stable sulfates were not formed (or to a smaller extent) and we have therefore described the sulfur species by $S1_{Cu}$–SO_2 and S2–SO_2 instead of sulfates. However, it should be noted that different sulfur species might be present on the copper sites and that the use of $S1_{Cu}$–SO_2 and S2–SO_2 was a simplification in order not to further complicate the model.

The results in Fig. 4 clearly show that there was an enhanced NH_3 storage after sulfur poisoning of the sample because of ammonia storage on these new sulfur sites [48]. Reactions (13) and (14) (see Table 4) were added to incorporate the reversible ammonia storage on these two sulfur species, $S1_{Cu}$–SO_2 and S2–SO_2, respectively. It is crucial to make these reactions reversible since it was observed that a similar amount of ammonia was adsorbed during repeated experiments and in addition, that the desorption peak during NH_3 TPD was magnified for the poisoned sample. However, by adding only these reactions, a similar amount of ammonia would be adsorbed in the model for the fresh as well as the poisoned sample because SO_2 attached to a Cu site that was previously an adsorption site for ammonia. During $NH_3 + SO_2 + O_2$ TPD, Zhang et al. [31] observed a stoichiometry of 2:1 of released NH_3 compared to SO_2 and to incorporate this finding, we introduced the possibility of attaching two ammonia molecules to each sulfur specie by adding Reactions (17) and (18) (see Table 4) on the two sulfur species. Since we likely did not have fully stable sulfates formed when using SO_2 compared to SO_3 during poisoning, the physical interpretation of these species was the formation and decomposition of ammonium sulfate precursors.

Another aspect that must be considered in the model is the gradual removal of sulfur species, as evident by the results in Fig. 5. Based on $NH_3 + SO_2 + O_2$ and $SO_2 + O_2$ TPD, Zhang et al. [31] found that a larger amount of sulfur was stored in the presence of ammonia. Further, some of the sulfur was released as SO_2 starting already at 300 °C, which is significantly lower than the $SO_2 + O_2$ TPD (SO_2 peaks at 550 and 680 °C). In addition, high temperature SO_2 peaks were also found for the $NH_3 + SO_2 + O_2$ TPD, showing that sulfur species with different binding strength existed on the catalyst. Our current model did not describe the fact that SO_2 was released earlier after poisoning had been performed in the presence of ammonia. We therefore introduced Reactions (15) and (16) (see Table 4) where the $S1_{Cu}$–SO_2–NH_3 and S2–SO_2–NH_3 could decompose to produce SO_2 and the adsorbed ammonia could thereafter desorb in Reactions 1-Cu, 1-Brön. and 2 (Table 3), respectively. By introducing this reversible reaction, SO_2 could also attach to ammonia on the copper sites, thereby describing the increased SO_2 storage observed when poisoning in the presence of NH_3.

The above described sulfur poisoning and regeneration model was used to simulate several experiments. Sulfur poisoning was performed only once, 90 min at 300 °C using 30 ppm SO_2, 400 ppm NH_3, 400 ppm NO, 8% O_2 and 5% H_2O. Thereafter, multiple experiments were conducted in the following order: SCR1, SCR2, SCR3, SCR4, SCR5, SCR6, SCR7, SCR8, NH_3 TPD and, finally, NH_3 oxidation. Since sulfur will be gradually removed during the first SCR experiments (see Fig. 5), it is important to simulate the poisoning and all experiments in one long sequence, as performed here. The result of the third SCR experiment after poisoning (SCR3) is shown in Fig. 6, in which both experimental as well as simulated NO, NH_3 and N_2O concentrations are depicted, in addition to the experiment and simulation of the fresh catalyst up to 300 °C. As described earlier, the steps at highest temperature were omitted from the graph for the fresh catalyst due to the shorter time intervals for these steps, but the results can be easily reviewed in Fig. 1. From the results in Fig. 6, it became evident that the SO_2 poisoning resulted in a severe deactivation of the NO_x reduction capacity. Further, at the start of the experiment at 100 °C, there was a total uptake of ammonia for a long time due to the large ammonia storage capacity of Cu/SSZ-13 and NO was simultaneously observed. At this low temperature, no conversion of the NO occurred. Thereafter, the temperature was increased to 125 °C and immediately, an NH_3 desorption peak became visible due to desorption of loosely bound ammonia. At this temperature, some NO_x reduction became also evident and experimentally, the NO_x conversion was increasing when the temperature increased and reached 100% conversion at 300–400 °C. The model well predicted the initial ammonia storage and the NO and NH_3 conversions up to 175 °C. However, the model over-predicted the conversion at 200 °C and simultaneously under-predicted the conversion at higher temperature. It is possible to tune the parameters for the sulfur removal and decrease those rates, which would improve the simulation results at 200 °C. However, this adjustment would also produce low conversions at lower temperatures and even worsen the results at high temperature. If instead the sulfur removal rates were increased, the results at high temperature would improve, albeit at the expense of the results at low temperature where high conversion would be seen in the model. Thus, using the current mechanism, it is not possible to describe the SCR activity after sulfur poisoning across the whole temperature interval from 100 to 400 °C.

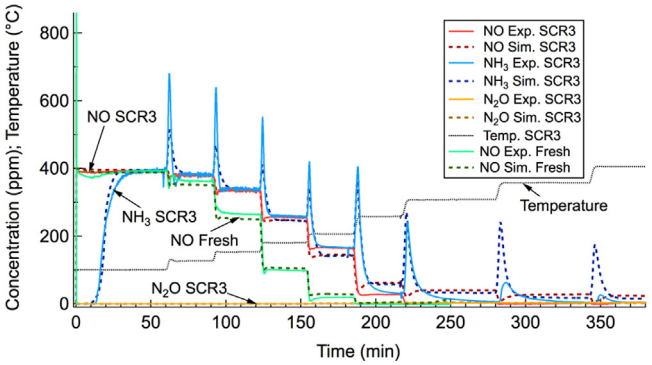

Fig. 6. Experiment and simulation of the third ammonia SCR experiment (SCR3) after sulfur poisoning. In addition, simulations for fresh catalyst up to 300 °C were added. The steps at highest temperature were omitted from the graph for fresh catalyst due to shorter time intervals for these steps, but the results can be easily reviewed in Fig. 1. The catalyst was exposed to 400 ppm NH_3, 400 ppm NO, 8% O_2 and 5% H_2O. Reaction (1) (Table 3), Reactions (2)–(10) (Table 1) and Reactions (11)–(18) (Table 4), were used.

Zhu et al. [68] observed NO_x reduction when exposing vanadia doped with NH_4HSO_4 to NO and O_2. Note that the only source of ammonia that could participate in the NO_x reduction was NH_4HSO_4. The reaction started at about 200 °C and exhibited a maximum above 300 °C. Interestingly, using pure NH_4HSO_4, only a minor NO_x reduction was visible below 400 °C. Accordingly, these

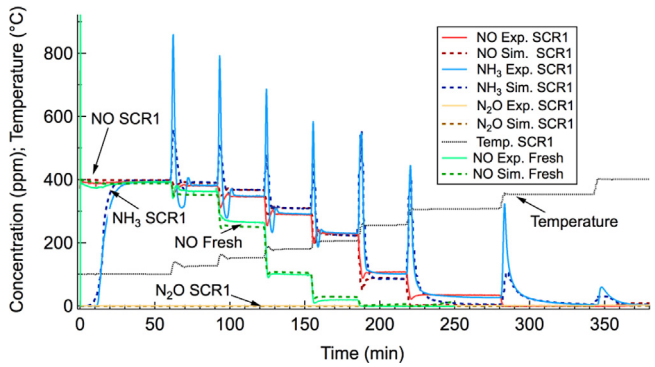

Fig. 7. Experiment and simulation of first ammonia SCR experiment (SCR1) after sulfur poisoning. In addition, simulations for the fresh catalyst up to 300 °C were added. The steps at highest temperature were omitted from the graph for the fresh catalyst due to shorter time intervals for these steps, but the results can be easily reviewed in Fig. 1. The catalyst was exposed to 400 ppm NH_3, 400 ppm NO, 8% O_2 and 5% H_2O. Reaction (1) (Table 3), Reactions (2)–(10) (Table 1) and Reactions (11)–(19) (Table 4), were used. The parameters used are given in Table 2 and Table 5.

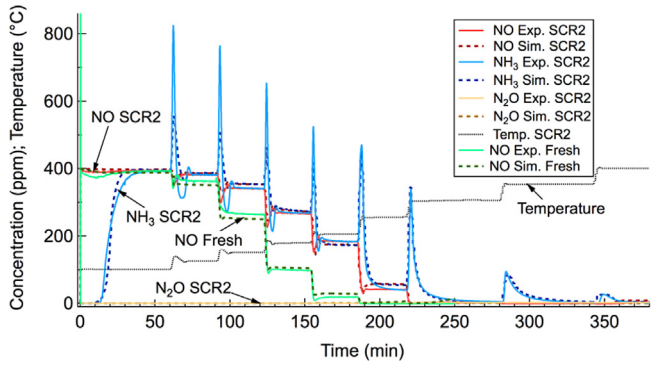

Fig. 8. Experiment and simulation of the second ammonia SCR experiment (SCR2) after sulfur poisoning. In addition, simulations for the fresh catalyst up to 300 °C were added. The steps at highest temperature were omitted from to the graph for the fresh catalyst due to shorter time intervals for these steps, but the results can be easily reviewed in Fig. 1. The catalyst was exposed to 400 ppm NH_3, 400 ppm NO, 8% O_2 and 5% H_2O. Reaction (1) (Table 3), Reactions (2)–(10) (Table 1) and Reactions (11)–(19) (Table 4), were used. The parameters used are given in Table 2 and Table 5.

results indicated that an interaction between the vanadia sites and the NH_4HSO_4 and NO seemed crucial. Based on the results presented by Zhu et al. [68] in combination with our simulation results shown in Fig. 6, we propose that ammonia attached to the copper-sulfur sites can also participate in the SCR reaction which is why Reaction (19) in Table 4 was added. In order not to further complicate the model, we only added one reaction for describing this process, but it would have been possible to add additional reactions.

The updated model using Reaction (1) (Table 3), Reactions (2)–(10) (Table 1) and Reactions (11)–(19) (Table 4), was used for the remaining simulations described in this paper. The parameters for these steps are given in Table 2 and Table 5. To further clarify, the results that will be presented in Figs. 7–12 were all performed in one simulation (Sulfur poisoning, SCR1, SCR2, SCR3, SCR4, SCR5, SCR6, SCR7, SCR8, NH_3 TPD, NH_3 oxidation) in order to capture the poisoning and gradual removal of the sulfur species. After the SO_2 poisoning at 300 °C under SCR conditions, an SCR experiment was conducted (SCR1) and the result from this experiment, together with its corresponding simulation, is shown in Fig. 7. In addition, the simulation and experiment of NO for the fresh catalyst up to 300 °C was added to the results to show the effect of the sulfur poisoning. The difference between NO for SCR1 and the fresh catalyst clearly showed that the deactivation was substantial and that the kinetic model well described this deactivation. The separation

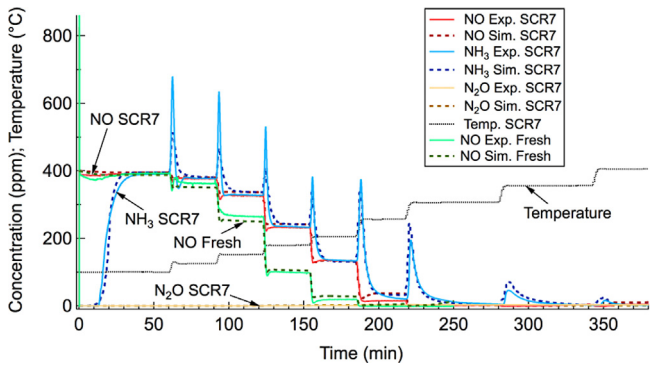

Fig. 9. Experiment and simulation of the seventh ammonia SCR experiment (SCR7) after sulfur poisoning. In addition, simulations for the fresh catalyst up to 300 °C were added. The steps at highest temperature were omitted from the graph for the fresh catalyst due to the shorter time intervals for these steps, but the results can be easily reviewed in Fig. 1. The catalyst was exposed to 400 ppm NH_3, 400 ppm NO, 8% O_2 and 5% H_2O. Reaction (1) (Table 3), Reactions (2)–(10) (Table 1) and Reactions (11)–(19) (Table 4), were used. The parameters used are given in Table 2 and Table 5.

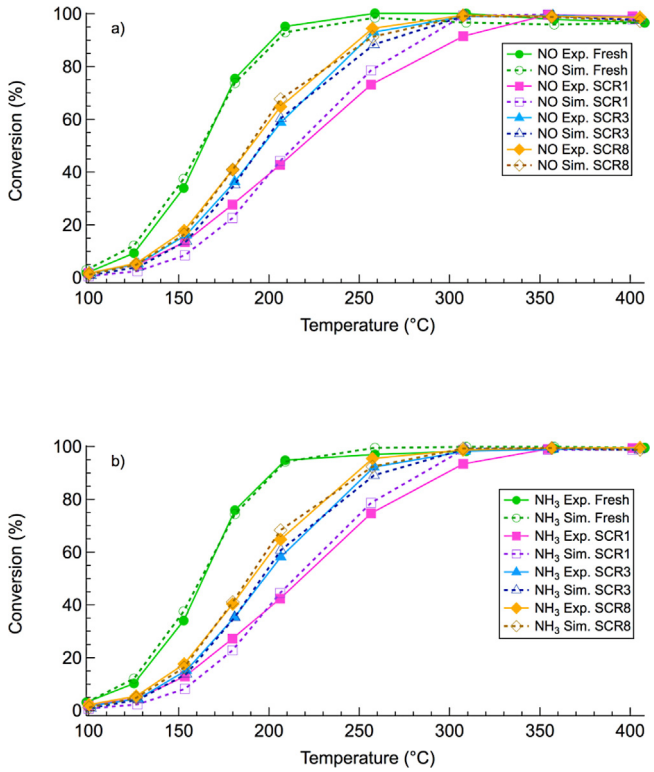

Fig.10. Experiment and simulation of SCR for the fresh catalyst and after sulfur poisoning (SCR, SCR3, SCR8). Steady state points for (a) NO and (b) NH_3 concentration. The catalyst was exposed to 400 ppm NH_3, 400 ppm NO, 8% O_2 and 5% H_2O. Reaction (1) (Table 3), Reactions (2)–(10) (Table 1) and Reactions (11)–(19) (Table 4), were used. The parameters used are given in Table 2 and Table 5.

of the copper and Brönsted acid sites in the S1 sites facilitated a correct description of the sulfur poisoning, which had not been possible in the simplified model shown in Fig. 3. In addition, the addition of Reaction (19) in Table 4 enabled a full conversion of NO at the highest temperatures, which would not have been achievable without this reaction (see Fig. 6).

After the SCR experiment shown in Fig. 7, this SCR experiment was repeated (SCR2) which resulted in an increased conversion as seen in Fig. 3. The reason for this increase was the removal of some sulfur species and the model was capable of capturing this regeneration very well, which was depicted in Fig. 8, where the results

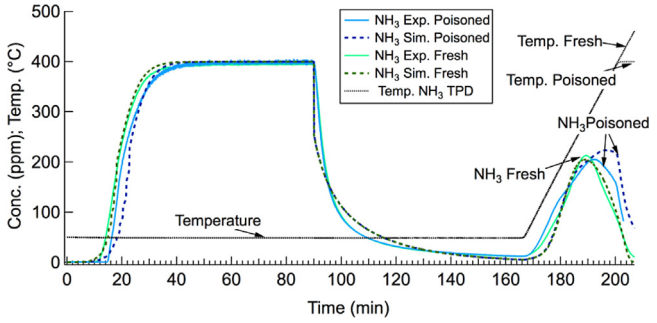

Fig. 11. Experiment and simulation of ammonia TPD after sulfur poisoning. In addition, an experiment of fresh conditions was added for comparison. The catalyst was exposed to 400 ppm NH_3, and 5% H_2O at 50 °C, followed by exposing the catalyst to 5% H_2O and, thereafter, increasing the temperature in a ramp. Reaction (1) (Table 3), Reactions (2)–(10) (Table 1) and Reactions (11)–(19) (Table 4), were used. The parameters used are given in Table 2 and Table 5.

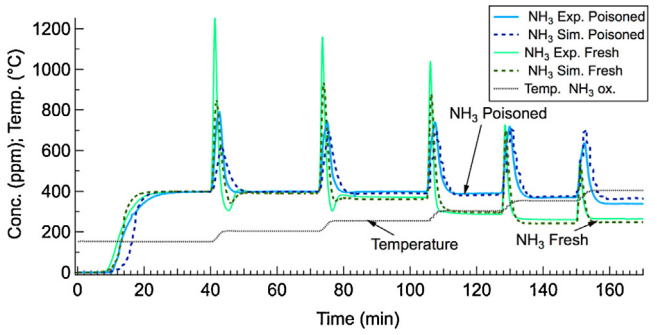

Fig. 12. Experiment and simulation of ammonia oxidation after sulfur poisoning. In addition, an experiment of fresh conditions was added for comparison. The catalyst was exposed to 400 ppm NH_3, 8% O_2 and 5% H_2O. Reaction (1) (Table 3), Reactions (2)–(10) (Table 1) and Reactions (11)–(19) (Table 4), were used. The parameters used are given in Table 2 and Table 5.

for SCR2 are shown. In addition, the model well described the initial ammonia storage at 100 °C, where the ammonia storage was increased due to storage on the new sulfur species, as shown in Fig. 4.

As is seen in Fig. 5, the activity recovery after sulfur removal was most clearly evident in the first few experiments after poisoning. Thereafter the activity leveled out and reached stable levels. This was a critical point that the model had to be capable of describing in order to predict the sulfur removal. The reason why some but not all of the sulfur was removed is probably because the sulfur species possess different binding strengths. Indeed, Zhang et al. [31] observed SO_2 release after $SO_2 + NH_3 + O_2$ exposure on Cu/SAPO-34 starting from slightly above 300 °C up to almost 800 °C. In order to incorporate these varying binding strengths into the model, a coverage dependent desorption, such as a Temkin isotherm, was used. This means that the activation energies for releasing sulfur from the ammonia sulfur species on copper (Reactions (15) and (16), Table 4) were increased when the coverage of different sulfur species decreased. By carefully tuning these coverage dependencies, the model was capable of capturing the initially high sulfur removal seen in SCR2, followed by a slower sulfur release and, finally, when steady state was reached. In Fig. 9, the results for the seventh repeated SCR experiments (SCR7) are shown and in this case, steady state conversions were received and no additional sulfur was removed. The model described the results of SCR7 very well, which showed that the sulfur removal model was functioning well.

To summarize the results from repeated SCR experiments, and to more easily visualize the effect of sulfur poisoning and its gradual removal, the conversions for the fresh catalyst, SCR1, SCR3 and SCR8 are shown in Fig. 10, where Fig. 10a shows NO conversions and Fig. 10b the NH_3 conversions. It is clearly seen that there was a large sulfur deactivation observed in the first SCR experiment after sulfur poisoning (SCR1). In the third SCR experiment (SCR3), some of the activity was regained. Finally, in the last SCR experiment (SCR8), only minor improvements in the conversion compared to SCR3 were observed, even though there were four more SCR experiments conducted in-between these two experiments. As described earlier, this took place because after several cycles, no more sulfur removal occurred. From the experimental and simulation results in Fig. 10, it became evident that the kinetic model developed described these experimental features very well.

After eight SCR experiment up to 400 °C, it became clear that no more sulfur would be released up to this temperature and additional experiments were performed. Both ammonia storage as well as ammonia oxidation experiments were conducted. The ammonia TPD experiment was simulated directly after the eight repeated SCR experiments (all simulations were performed in one sequence). In this experiment, the catalyst was exposed to 400 ppm NH_3 and 5% H_2O at 50 °C, followed by the sample being flushed with 5% H_2O in Ar. Thereafter, using a ramp speed of 10 °C/min, the temperature was increased to 400 °C. The results from the NH_3 TPD for the fresh catalyst as well as after sulfur poisoning are shown in Fig. 11. Initially, there was a large total uptake of ammonia due to the large ammonia storage capacity of Cu/SSZ-13. The ammonia storage was larger for the sulfur-poisoned sample, which was described by the model due to the attachment of up to two ammonia molecules to the sulfur species on the copper sites. Further, when the ammonia was turned off, loosely bound ammonia was desorbed and when the temperature was increased, a large desorption peak became visible. The sulfur poisoned sample exhibited additional ammonia desorption at high temperature, which the model could also adequately capture. Note that the temperature ramp after sulfur poisoning was only up to 400 °C and thereafter the temperature leveled out, but for the fresh catalyst, the ramp was up to 600 °C. This is the reason for the sudden change in slope for the ammonia concentration of the poisoned sample at about 200 min. Furthermore, the increased ammonia storage on the copper-sulfur species can also be seen by examining the desorption peaks in the repeated SCR experiments, when increasing the temperature. For example, the ammonia desorption peak occurring at about 155 min in the experiments shown in Figs. 6–9 is significantly higher for SCR1 (Fig. 7) and SCR2 (Fig. 8) compared to SCR3 (Fig. 6) and SCR7 (Fig. 9). This can be explained by the larger amount of sulfur species on SCR1 and SCR2, and thereby more available sites for ammonia storage.

The final experiment simulated in the sequence was the ammonia oxidation. In this experiment, the catalyst was exposed to 400 ppm NH_3, 8% O_2 and 5% H_2O and the temperature was stepwise increased from 150 to 400 °C. The results from the simulation and experiment are shown in Fig. 12, together with results for the fresh catalyst. Even for the fresh catalyst, the ammonia oxidation activity was quite low. This was because the sample was under-exchanged with copper [12] and it was previously observed that copper zeolites with low copper-loading exhibited low ammonia and NO oxidation rates [20]. The ammonia oxidation reaction was severely deactivated for the sulfur-poisoned sample and the model was also capable of describing this experiment very well.

5. Conclusions

In this study, we have developed a kinetic model used for ammonia SCR applications to describe the sulfur poisoning and gradual sulfur removal over Cu/SSZ-13. A three-site kinetic model, previously developed for a fresh catalyst, was used as a base. This catalyst

was under-exchanged in Cu, and based on a thorough characterization of Cu/SSZ-13 in the literature, it is likely that the copper was primarily located in the six-membered rings. These sites are represented by S1 in the model. When the copper loading was increased, Cu was thereafter located in the larger cages or formed Cu_xO_y species and we have these species in the model by S2. The Brönsted sites could also adsorb ammonia and in order to simplify the model, they were lumped together with the S1 and S2 sites. Finally, S3 was a site where physisorbed ammonia could attach at low temperature. The model for the fresh catalyst included ammonia adsorption/desorption, ammonia oxidation, ammonia SCR and N_2O formation. A maximum in N_2O formation was observed at low temperature and reactions steps including NH_3–NO intermediate species on the copper sites was included. Furthermore, the N_2O formation again increased at high temperature and therefor was one additional reaction step added to describe this feature.

After the experiments using a fresh catalyst had been conducted, the sample was sulfur poisoned at 300 °C for 90 min under SCR conditions. Thereafter, eight repeated SCR experiments, denoted SCR1, SCR2, etc., were conducted in order to examine the effect of sulfur poisoning and gradual regeneration. Note that sulfur poisoning was only conducted one time, before all eight SCR experiments. A large deactivation after sulfur poisoning (SCR1) was observed. After repeated SCR experiments, parts of the sulfur were gradually removed, but after a few cycles, a stable activity, which was significantly lower than the original activity, was reached. After these repeated SCR experiments, additional experiments were performed including NH_3 TPD and NH_3 oxidation. Since sulfur during some of the experiments was gradually removed; all experiments were simulated starting from the sulfur poisoning in one long sequence.

A simple model with SO_2 adsorbing on S1 and S2 was first examined. However, even though almost complete uptake in the model was received, the deactivation was still too low compared to the experiment. We suggest that the reason for the poor functionality of this initial model was because we lumped the Brönsted acid sites together with the copper sites in the model, but the sulfur was likely in reality preferentially adsorbed on the copper sites. In the updated model, we therefore divided the S1 sites into $S1_{Cu}$ and $S1_{Brön.}$ and enabled only SO_2 adsorption on the $S1_{Cu}$ site. It would have been possible to use the same approach for S2 as well, but since the site density for S2 was already quite low, it was not crucial to the model and was therefore omitted in order not to further complicate the model. It should be noted that all experiments were conducted in the presence of water, and the copper sites are therefore likely hydrated, thus $S1_{Cu}$ and S2 sites represents hydrated sites.

The first steps in the sulfur model were the adsorption of SO_2 to $S1_{Cu}$ and S2. Experimentally, it was observed that there was a larger ammonia storage occurring after sulfur poisoning than for the fresh catalyst. In the kinetic model, ammonia adsorption and desorption on the $S1_{Cu}$–SO_2 and S2–SO_2 sites were therefore enabled. However, since ammonia was already being adsorbed to the copper site, if only one ammonia molecule was attached to each of these sites, it would have resulted in similar ammonia storage. Hence, $S1_{Cu}$–SO_2–$(NH_3)_2$ and S2–SO_2–$(NH_3)_2$ species formation and decomposition were added to the model, where these species represented precursors to ammonium sulfate formation. In the literature, it was observed that TPD experiments with $SO_2 + NH_3 + O_2$ resulted in the release of SO_2 at significantly lower temperature than $SO_2 + O_2$ TPD. In order to incorporate this feature into the model, reversible steps were added to the model where the $S1_{Cu}$–SO_2–NH_3 and S2–SO_2-NH_3 species were decomposed to form SO_2. Finally, a reaction step was added to describe the SCR reaction between $S1_{Cu}$–SO_2–$(NH_3)_2$ species with NO. This step was necessary in order to describe the experimental features over the entire temperature range examined. The developed model could well describe the sulfur poisoning and gradual regeneration during repeated SCR experiments. In addition, the model was used to simulate NH_3 TPD and NH_3 oxidation and for these cases, the model could also well describe the experimental findings before and after sulfur poisoning.

Acknowledgments

This study was performed at the Competence Centre for Catalysis, Chemical Engineering at Chalmers University and Cummins Inc. The financial support of Cummins Inc. and the Swedish Research Council (621-2011-4860 and 642-2014-5733) are gratefully acknowledged.

References

[1] I. Nova, L. Lietti, E. Tronconi, P. Forzatti, Transient response method applied to the kinetic analysis of the DeNO(x)-SCR reaction, Chem. Eng. Sci. 56 (2001) 1229–1237.
[2] B. Roduit, A. Wokaun, A. Baiker, Global kinetic modeling of reactions occurring during selective catalytic reduction of NO by NH3 over vanadia/titania-based catalysts, Ind. Eng. Chem. Res. 37 (1998) 4577–4590.
[3] J.A. Dumesic, N.-Y. Topsoe, H. Topsoe, Y. Chen, T. Slabiak, Kinetics of selective catalytic reduction of nitric oxide by ammonia over Vanadia/Titania, J. Catal. 163 (1996) 409–417.
[4] L. Lietti, I. Nova, E. Tronconi, P. Forzatti, Catal. Today 45 (1998).
[5] D. Chatterjee, T. Burkhardt, M. Weibel, E. Tronconi, I. Nova, C. Ciardelli, Numerical simulation of NO/NO2/NH3 reactions on SCR-catalytic converters: model development and applications, SAE (2006), 2006-01-0468.
[6] S. Malmberg, M. Votsmeier, J. Gieshoff, N. Söger, L. Mußmann, A. Schuler, A. Drochner, Dynamic phenomena of SCR-catalysts containing Fe-exchanged zeolites—experiments and computer simulations, Top. Catal. 42–43 (2007) 33–36.
[7] D. Chatterjee, T. Burkhardt, M. Weibel, I. Nova, A. Grossale, E. Tronconi, Numerical simulation of Zeolite- and V-based SCR catalytic converters, SAE (2007), 2007-01-1136.
[8] H. Sjovall, R.J. Blint, A. Gopinath, L. Olsson, A kinetic model for the selective catalytic reduction of NOx with NH3 over an Fe-zeolite catalyst, Ind. Eng. Chem. Res. 49 (2010) 39–52.
[9] J.H. Kwak, H.Y. Zhu, J.H. Lee, C.H.F. Peden, J. Szanyi, Two different cationic positions in Cu-SSZ-13? Chem. Commun. 48 (2012) 4758–4760.
[10] S.A. Bates, A.A. Verma, C. Paolucci, A.A. Parekh, T. Anggara, A. Yezerets, W.F. Schneider, J.T. Miller, W.N. Delgass, F.H. Ribeiro, Identification of the active Cu site in standard selective catalytic reduction with ammonia on Cu-SSZ-13, J. Catal. 312 (2014) 87–97.
[11] K. Wijayanti, S. Andonova, A. Kumar, J. Li, K. Kamasamudram, N.W. Currier, A. Yezerets, L. Olsson, Impact of sulfur oxides on ammonia SCR over CukSAPO-34, Appl. Catal. B: Environ. 166–167 (2015) 568.
[12] L. Olsson, K. Wijayanti, K. Leistner, A. Kumar, S. Joshi, K. Kamasamudram, N.W. Currier, A. Yezerets, A multi-site kinetic model for NH3-SCR over Cu/SSZ-13, Appl. Catal. B: Environ. 174–175 (2015) 212.
[13] N. Wilken, K. Wijayanti, K. Kamasamudram, N.W. Currier, R. Vedaiyan, A. Yezerets, L. Olsson, Mechanistic investigation of hydrothermal aging of Cu-Beta for ammonia SCR, Appl. Catal. B 111 (2012) 58.
[14] K. Kamasamudram, N.W. Currier, X. Chen, A. Yezerets, Overview of the practically important behaviors of zeolite-based urea-SCR catalysts, using compact experimental protocol, Catal. Today 151 (2010) 212–222.
[15] S.J. Schmieg, S.H. Oh, C.H. Kim, D.B. Brown, C.H.F. Lee, D.H. Kim, Thermal durability of Cu-CHA NH3-SCR catalysts for diesel NOx reduction, Catal. Today 184 (2012) 252–261.
[16] L. Wang, W. Li, G.S. Qi, D. Weng, Location and nature of Cu species in Cu/SAPO-34 for selective catalytic reduction of NO with NH3, J. Catal. 289 (2012) 21–29.
[17] K. Leistner, O. Mihai, K. Wijayanti, A. Kumar, K. Kamasamudram, N.W. Currier, A. Yezerets, L. Olsson, Comparison of Cu/BEA, Cu/SSZ-13 and Cu/SAPO-34 for ammonia-SCR reactions, Catal. Today (2015), http://dx.doi.org/10.1016/j.cattod.2015.04.004.
[18] D.W. Fickel, E. D'Addio, J.A. Lauterbach, R.F. Lobo, The ammonia selective catalytic reduction activity of copper-exchanged small-pore zeolites, Appl. Catal. B-Environ. 102 (2011) 441–448.
[19] A.M. Beale, F. Gao, I. Lezcano-Gonzalez, C.H.F. Peden, J. Szanyi, Recent advances in automotive catalysis for NOx emission control by small-pore microporous materials, Chem. Soc. Rev. 44 (2015) 7371.
[20] O. Mihai, C. Widyastuti, S. Andonova, K. Kamasamudram, J. Li, S. Joshi, N.W. Currier, A. Yezerets, L. Olsson, The effect of Cu-loading on the reactions involved in ammonia SCR over Cu zeolites, J. Catal. 311 (2014) 170.
[21] A.A. Verma, S.A. Bates, T. Anggara, C. Paolucci, A.A. Parekh, K. Kamasamudram, A. Yezerets, J.T. Miller, W.N. Delgass, W.F. Schneider, F.H. Ribeiro, NO oxidation: a probe reaction on Cu-SSZ-13, J. Catal. 312 (2014) 179–190.

[22] U. Deka, A. Juhin, E.A. Eilertsen, H. Emerich, M.A. Green, S.T. Korhonen, B.M. Weckhuysen, A.M. Beale, Confirmation of isolated Cu2+ Ions in SSZ-13 zeolite as active sites in NH3-selective catalytic reduction, J. Phys. Chem. C 116 (2012) 4809–4818.
[23] D.W. Fickel, J.M. Fedeyko, R.F. Lobo, Copper coordination in Cu–SSZ-13 and Cu–SSZ-16i nvestigated by variable-temperature XRD, J. Phys. Chem. C 114 (2010) 1633–1640.
[24] F. Gao, E.D. Walter, E.M. Karp, J.Y. Luo, R.G. Tonkyn, J.H. Kwak, J. Szanyi, C.H.F. Peden, Structure-activity relationships in NH3-SCR over Cu-SSZ-13 as probed by reaction kinetics and EPR studies, J. Catal. 300 (2013) 20–29.
[25] S.J. Schmieg, J.-H. Lee, Evaluation of supplier catalyst formulations for the selective catalytic reduction of NOx with ammonia, SAE (2005), 2005-01-3881.
[26] J.W. Girard, C. Montreuil, J. Kim, G. Cavataio, C. Lambert, Technical advantages of vanadium SCR systems for diesel NOx control in emerging markets, SAE Int. J. Fuels Lubr. 1 (2008) 488–494.
[27] J.A. Ura, J. Girard, G. Cavataio, C. Montreuil, C. Lambert, Cold start performance and enhanced thermal durability of vanadium SCR catalysts, SAE (2009), 2009-01-0625.
[28] G. Cavataio, J. Girard, J.E. Patterson, C. Montreuil, Y. Cheng, C.K. Lambert, Laboratory testing of urea-SCR formulations to meet Tier 2 Bin 5 emissions, SAE (2007), 2007-01-1575.
[29] Y. Cheng, C. Montreuil, G. Cavataio, C. Lambert, Sulfur tolerance and DeSOx studies on diesel SCR catalysts, SAE Int. J. Fuels Lubr. 1 (2008) 471–476.
[30] L. Zhang, D. Wang, Y. Liu, K. Kamasamudram, J. Li, W. Epling, SO2 poisoning impact on the NH3-SCR reaction over a commercial Cu-SAPO-34 SCR catalyst, Appl. Catal. B-Environ. 156 (2014) 371–377.
[31] L. Zhang, D. Wang, Y. Liu, K. Kamasamudram, J.H. Li, W. Epling, SO2 poisoning impact on the NH3-SCR reaction over a commercial Cu-SAPO-34 SCR catalyst, Appl. Catal. B-Environ. 156 (2014) 371–377.
[32] A. Kumar, M.A. Smith, K. Kamasamudram, N.W. Currier, H. An, A. Yezerets, Impact of different forms of feed sulfur on small-pore Cu-zeolite SCR catalyst, Catal.Today 231 (2014) 75–82.
[33] L. Olsson, H. Sjovall, R.J. Blint, A kinetic model for ammonia selective catalytic reduction over Cu-ZSM-5, Appl. Catal. B 81 (2008) 203–217.
[34] L. Olsson, H. Sjövall, R.J. Blint, Detailed kinetic modeling of NOx adsorption and NO oxidation over Cu-ZSM-5, Appl. Catal. B: Environ. 87 (2009) 200.
[35] H. Sjövall, L. Olsson, R.J. Blint, Detailed kinetic modeling of NH3 adsorption and NH3 oxidation over Cu-ZSM-5, J. Phys. Chem. C 113 (2009) 1393.
[36] H. Sjövall, R.J. Blint, L. Olsson, Detailed kinetic modeling of NH3 SCR over Cu-ZSM-5, Appl. Catal. B 92 (2009) 138.
[37] G. Delahay, S. Kieger, N. Tanchoux, P. Trens, B. Coq, Kinetics of the selective catalytic reduction of NO by NH3 on a Cu-faujasite catalyst, Appl. Catal. B: Environ. 52 (2004) 251–257.
[38] Supriyanto, K. Wijayanti, A. Kumar, S. Joshi, K. Kamasamudram, N.W. Currier, A. Yezerets, L. Olsson, A global kinetic model for hydrothermal aging of Cu zeolites used in NH3 SCR, Appl. Catal. B: Environ. 163 (2015) 382.
[39] P.S. Metkar, M.P. Harold, V. Balakotaiah, Experimental and kinetic modeling study of NH3-SCR of NOx on Fe-ZSM-5, Cu-chabazite and combined Fe- and Cu-zeolite monolithic catalysts, Chem. Eng. Sci. 87 (2013) 51–66.
[40] S.A. Stevenson, J.C. Vartuli, C.F. Brooks, Kinetics of the selective catalytic reduction of NO over HZSM-5, J. Catal. 190 (2000) 228–239.
[41] M. Colombo, I. Nova, E. Tronconi, V. Schmeisser, B. Bandl-Konrad, L. Zimmermann, NO/NO2/N2O-NH3 SCR reactions over a commercial Fe-zeolite catalyst for diesel exhaust aftertreatment: intrinsic kinetics and monolith converter modelling, Appl. Catal. B-Environ. 111 (2012) 106–118.
[42] J.H. Baik, S.D. Yim, I.S. Nam, Y.S. Mok, J.H. Lee, B.K. Cho, S.H. Oh, Modeling of monolith reactor washcoated with CuZSM5 catalyst for removing NO from diesel engine by urea, Ind. Eng. Chem. Res. 45 (2006) 5258–5267.
[43] A. Grossale, I. Nova, E. Tronconi, D. Chatterjee, M. Weibel, NH3-NO/NO2 SCR for diesel exhausts aftertreatment: reactivity, mechanism and kinetic modelling of commercial Fe- and Cu-promoted zeolite catalysts, Top. Catal. 52 (2009) 1837–1841.
[44] N. Wilken, K. Kamasamudram, N.W. Currier, J. Li, A. Yezerets, L. Olsson, Heat of adsorption for NH3, NO2 and NO on Cu-Beta zeolite using microcalorimeter for NH3 SCR applications, Catal. Today 151 (2010) 237–243.
[45] E. Tronconi, I. Nova, C. Ciardelli, D. Chatterjee, B. Bandl-Konrad, T. Burkhardt, Modelling of an SCR catalytic converter for diesel exhaust after treatment: dynamic effects at low temperature, Catal. Today 105 (2005) 529–536.
[46] M. Colombo, G. Koltsakis, I. Nova, E. Tronconi, Modelling the ammonia adsorption-desorption process over an Fe-zeolite catalyst for SCR automotive applications, Catal. Today 188 (2012) 42–52.
[47] S.A. Skarlis, D. Berthout, A. Nicolle, C. Dujardin, P. Granger, IR spectroscopy analysis and kinetic modeling study for NH3 adsorption and desorption on H- and Fe-BEA Catalysts, J. Phys. Chem. C 117 (2013) 7154–7169.
[48] K. Wijayanti, S. Andonova, A. Kumar, J. Li, K. Kamasamudram, N.W. Currier, A. Yezerets, L. Olsson, Deactivation study of Cu-SSZ-13 by SO2 in SCR condition used for NH3-SCR, Submitted., (2015).
[49] AVL BOOST Aftertreatment Manual, AVL, 2009. <http://www.avl.com>.
[50] D. Chatterjee, T. Burkhardt, B. Bandl-Konrad, T. Braun, E. Tronconi, I. Nova, C. Ciardelli, Numerical simulation of ammonia SCR-catalytic converters: model development and application, SAE (2005), 2005-01-0965.
[51] H. Sjövall, L. Olsson, E. Fridell, R.J. Blint, Selective catalytic reduction of NOx with NH3 over Cu-ZSM-5—The effect of changing the gas composition, Appl. Catal. B 64 (2006) 180.
[52] L. Olsson, Kinetic Modeling of Ammonia SCR for Cu-Zeolite Catalysts, (2014) 357–382.
[53] M. Colombo, I. Nova, E. Tronconi, Detailed kinetic modeling of the NH3-NO/NO2 SCR reactions over a commercial Cu-zeolite catalyst for diesel exhausts after treatment, Catal. Today 197 (2012) 243–255.
[54] A. Pant, S.J. Schmieg, Kinetic model of NOx SCR using urea on commercial Cu-Zeolite catalyst, Ind. Eng. Chem. Res. 50 (2011) 5490–5498.
[55] I. Nova, D. Bounechada, R. Maestri, E. Tronconi, A.K. Heibel, T.A. Collins, T. Boger, Influence of the substrate properties on the performances of NH3-SCR monolithic catalysts for the aftertreatment of diesel exhaust: an experimental and modeling study, Ind. Eng. Chem. Res. 50 (2011) 299–309.
[56] T.C. Watling, M.R. Ravenscroft, G. Avery, Catal. Today 188 (2012) 32.
[57] K. Leistner, F. Brüsewitz, K. Wijayanti, A. Kumar, J. Li, K. Kamasamudram, N.W. Currier, A. Yezerets, L. Olsson, Impact of Copper Loading on NH3-SCR and Related Reactions over Cu/SAPO-34, In manuscript., (2015).
[58] N. Wilken, R. Nedyalkova, K. Kamasamudram, J. Li, N.W. Currier, R. Vedaiyan, A. Yezerets, L. Olsson, Investigation of the effect of accelerated hydrothermal aging on the Cu sites in a Cu-BEA catalyst for NH3-SCR applications, Top. Catal. 56 (2013) 317–322.
[59] J.S. McEwen, T. Anggara, W.F. Schneider, V.F. Kispersky, J.T. Miller, W.N. Delgass, F.H. Ribeiro, Integrated operando X-ray absorption and DFT characterization of Cu-SSZ-13 exchange sites during the selective catalytic reduction of NOx with NH3, Catal. Today 184 (2012) 129–144.
[60] F. Giordanino, E. Borfecchia, K.A. Lomachenko, A. Lazzarini, G. Agostini, E. Gallo, A.V. Soldatov, P. Beato, S. Bordiga, C. Lamberti, Interaction of NH3 with Cu-SSZ-13 catalyst: a complementary FTIR, XANES, and XES Study, J. Phys. Chem. Lett. 5 (2014) 1552–1559.
[61] M. Moreno-Gonzalez, B. Hueso, M. Boronat, T. Blasco, A. Corma, Ammonia-containing species formed in Cu-Chabazite as per In situ EPR, solid-state NMR, and DFT calculations, J. Phys. Chem. Lett. 6 (2015) 1011–1017.
[62] R. Nedyalkova, K. Kamasamudram, N.W. Currier, J. Li, A. Yezerets, L. Olsson, Experimental evidence of the mechanism behind NH3 overconsumption during SCR over Fe-zeolites, J. Catal. 299 (2013) 101.
[63] O. Mihai, C.R. Widyastuti, A. Kumar, J. Li, S.Y. Joshi, K. Kamasamudram, N.W. Currier, A. Yezerets, L. Olsson, The effect of NO2/NOx feed ratio on the NH3-SCR system over Cu-zeolites with varying loading, Catal. Lett. 144 (1) (2014) 70.
[64] G. Delahay, B. Coq, S. Kieger, B. Neveu, The origin of N2O formation in the selective catalytic reduction of NOx by NH3 in O2 rich atmosphere on Cu-faujasite catalysts, Catal. Today 54 (1999) 431.
[65] G. Centi, S. Perathoner, D. Biglino, E. Giamello, J. Catal. 151 (1995) 75.
[66] I. Lezcano-Gonzalez, U. Deka, B. Arstad, A. Van Yperen-De Deyne, K. Hemelsoet, M. Waroquier, V. Van Speybroeck, B.M. Weckhuysen, A.M. Beale, Determining the storage, availability and reactivity of NH3 within Cu-Chabazite-based ammonia selective catalytic reduction systems, Phys. Chem. Chem. Phys. 16 (2014) 1639–1650.
[67] M. Shen, H. Wen, T. Hao, T. Yu, D. Fan, J. Wang, W. Li, J. Wang, Deactivation mechanism of SO2 on Cu/SAPO-34 NH3-SCR catalysts: structure and active Cu2+, Catal. Sci. Technol. 5 (3) (2015) 1741–1749.
[68] Z. Zhu, H. Niu, Z. Liu, S. Liu, Decomposition and reactivity of NH4HSO4 on V2O5/AC catalysts used for NO reduction with ammonia, J. Catal. 195 (2000) 268–278.